Confinement engineering of *s-d* exchange interactions in $Ga_{1-x}Mn_xAs/Al_yGa_{1-y}As$ quantum wells

N. P. Stern, R. C. Myers, M. Poggio, A. C. Gossard, and D. D. Awschalom
Center for Spintronics and Quantum Computation, University of California, Santa Barbara, California 93106, USA
(Received 21 April 2006; revised manuscript received 26 October 2006; published 19 January 2007)

Recent measurements of coherent electron spin dynamics reveal an antiferromagnetic *s-d* exchange coupling between conduction-band electrons and electrons localized on Mn^{2+} impurities in $Ga_{1-x}Mn_xAs$ quantum wells. Here we discuss systematic measurements of the *s-d* exchange interaction in $Ga_{1-x}Mn_xAs/Al_yGa_{1-y}As$ quantum wells with different confinement potentials using time-resolved Kerr rotation. Extending previous investigations of the dependence of the *s-d* exchange, $N_0\alpha$, on well width, we find that its magnitude also depends on well depth. Both phenomena reduce to a general dependence on confinement energy, described by a band-mixing model of confinement-induced kinetic exchange in the conduction band.

DOI: 10.1103/PhysRevB.75.045329 PACS number(s): 75.30.Et, 75.50.Pp, 78.47.+p, 71.70.Gm

Dilute magnetic semiconductors (DMS) are a scientifically and technologically interesting class of materials due to the strong *sp-d* exchange interactions between the *s*-like conduction band or the *p*-like valance band and the localized *d* shell of magnetic dopants.[1] The strength of these couplings and the resulting enhancement of Zeeman spin splittings lead to dramatic spin-dependent properties in DMS including the formation of magnetic polarons,[1,2] the coherent transfer of spin polarization from carriers to magnetic ions,[3] and carrier-mediated ferromagnetism.[4] Heterostructures with DMS layers offer the freedom to engineer exchange spin splittings of carriers in electronic devices.[5] The exchange interactions in II-VI DMS have been characterized by band-edge magneto-optical spectroscopy[6,7] and are well understood theoretically.[8,9] Measurements in II-VI DMS quantum wells (QWs) reveal that increasing quantum confinement reduces the strength of the *s-d* exchange due to kinetic exchange effects,[10–12] suggesting additional avenues for manipulating carrier exchange interactions in DMS heterostructures using band engineering.

Comparable studies in III-V alloys such as $Ga_{1-x}Mn_xAs$ have been more difficult because of the high defect densities in normal growth conditions. Recent refinements of molecular-beam epitaxy (MBE) techniques allow production of high-quality III-V paramagnetic DMS heterostructures allowing optical measurement of exchange interactions through electron spin coherence.[13,14] The *s-d* exchange constant $N_0\alpha$ was observed to be antiferromagnetic in $Ga_{1-x}Mn_xAs$ QWs, rather than ferromagnetic as concluded in earlier magneto-optical studies in bulk $Ga_{1-x}Mn_xAs$.[15,16] Despite the difference in the sign of the interaction in $Ga_{1-x}Mn_xAs$ QWs as compared with II-VI QWs,[12] the data show that $N_0\alpha$ decreases with increasing one-dimensional (1D) quantum confinement in both materials. Here we extend previous measurements of $N_0\alpha$ in $Ga_{1-x}Mn_xAs/Al_yGa_{1-y}As$ QWs by additionally varying the QW barrier height, which confirms this dependence on quantum confinement.

Single $Ga_{1-x}Mn_xAs/Al_yGa_{1-y}As$ quantum wells of width d are grown by MBE on (001) semi-insulating GaAs wafers using the conditions outlined in Ref. 14. QWs with barriers containing different fractions of Al (y) are grown in which the QW barrier height E_b is proportional to y. In particular, we grow samples with $y=0.1$ and $d=10$ nm, with $y=0.2$ and $d=10$ nm, and with $y=0.2$ and $d=5$ nm. Figure 1(a) depicts the energy diagram for these structures, where the electron kinetic energy E_e is defined as the energy between the bottom of the GaAs conduction band and the ground-state energy in the QW. E_e is calculated from the material and structural parameters of the QWs using a one-dimensional Poisson-Schrödinger solver.[17] These structures complement the four QWs measured for $y=0.4$ and $d=3$, 5, 7.5, and 10 nm in Ref. 13. The variation of the QW depth allows E_e to be varied independently from d, addressing the possibility that d-dependent parameters aside from E_e affect $N_0\alpha$. By varying y, we circumvent possible changes in the measured $N_0\alpha$ due to different Mn incorporation behavior or Mn-profile measurement artifacts related to QW width.

For each aforementioned y and d pair, we measure a sample set consisting of a nonmagnetic control sample ($x=0$) and four samples with increasing Mn doping ($0.000\,02<x<0.0007$), for a total of 15 samples. The effective Mn doping level x is determined quantitatively by secondary ion mass spectroscopy (SIMS) as described in Ref. 14. Figure 1(b) shows a typical Mn doping profile obtained by SIMS for $d=10$ nm QWs. The Mn profiles in the QW region exhibit no appreciable dependence on the Al concentration, indicating that QWs of different y have similar Mn incorporation behavior.

We observe photoluminescence from both the band-edge

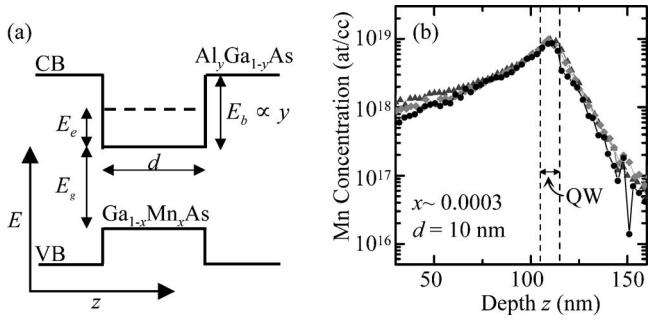

FIG. 1. (a) Schematic of the QW band structure, showing the well width d, the GaAs band gap E_g, the QW barrier height E_b, and the electron kinetic energy E_e. (b) SIMS Mn profiles for three $d=10$ nm QWs for nominally the same Mn concentration $x\sim 0.0003$, with $y=0.1$ (light gray), 0.2 (gray), and 0.4 (black).

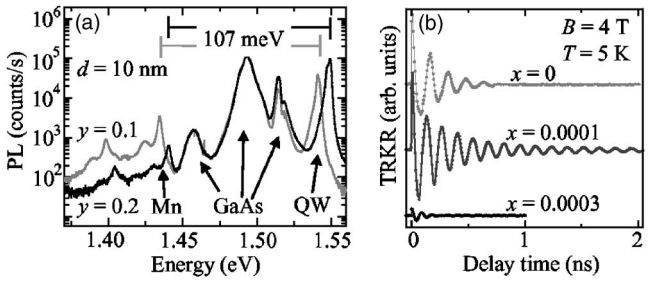

FIG. 2. (a) PL spectra from $d=10$ nm QWs where the Mn acceptor peak is shifted ~107 meV lower in energy than the QW PL. The $y=0.1$, $x=0.000\,05$ (gray) and $y=0.2$, $x=0.000\,03$ (black) QWs are shown. (b) KR from $d=5$ nm, $y=0.2$ QWs demonstrating increasing spin precession frequency with higher Mn doping and an enhanced transverse spin lifetime with light Mn doping, which decreases with higher doping.

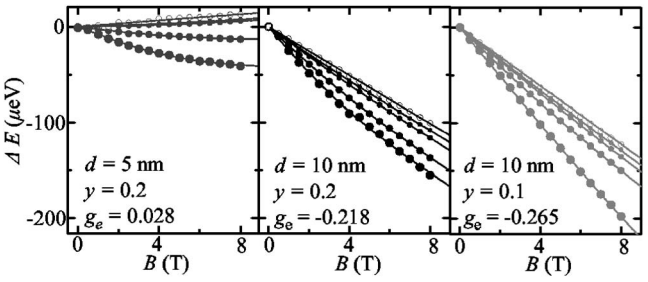

FIG. 3. Spin splittings extracted from KR for $d=10$ nm, $y=0.1$ (gray), $d=10$ nm, $y=0.2$ (black), and $d=5$ nm, $y=0.2$ (light gray) with increased dot size representing higher Mn concentration. Nonmagnetic control samples (open symbols) give the electron g factor used in the spin-$\frac{5}{2}$ paramagnetism fits (solid lines) (Ref. 13).

exciton and the Mn acceptor [Fig. 2(a)]. The Mn luminescence is redshifted by 0.107 eV from the QW band edge, consistent with the Mn ionization energy measured in $GaAs/Al_{1-x}Ga_xAs$ superlattices.[18]

Measurements of $N_0\alpha$ are made using results from both time-resolved Kerr rotation (KR) and SIMS as described in Myers *et al.*[13] and Poggio *et al.*[14] Pulses from a mode-locked Ti:sapphire laser with 76-MHz repetition rate are split into pump and probe beams with average powers of 2 and 0.1 mW, respectively; the beams are focused to an overlapping spot on the sample with the laser propagation direction perpendicular to the external magnetic field B (x axis) and parallel to the QW growth axis (z axis). Changes in the linear polarization angle (measured as KR) of the reflected probe beam are measured as a function of the time delay between the two pulses, producing a signal proportional to the pump-induced electron spin polarization. Fits to a decaying cosine function yield the transverse spin coherence time T_2^* and the electron Larmor precession frequency ν_L [Fig. 2(b)]. As observed in Ref. 14, light Mn doping increases T_2^* within each (d,y) set. Using the methods of Refs. 13 and 14, the ν_L are converted to spin splittings ΔE, which are fit to $\Delta E=g_e\mu_B B-xN_0\alpha\langle S_x\rangle$, where g_e is the in-plane electron g factor, μ_B is the Bohr magneton, and $\langle S_x\rangle$ is the spin of the paramagnetic Mn system along the applied field. In this way, a single value for $N_0\alpha$ is extracted for each (d,y) sample set from the KR (Fig. 3).

Plots of $N_0\alpha$ as a function of y for $d=5$ and 10 nm (Fig. 4, inset) show that for constant d, a larger barrier height leads to a more negative exchange constant. We plot $N_0\alpha$ as a function of E_e in Fig. 4. The s-d exchange becomes more antiferromagnetic with increasing E_e; this holds equally well for variation in E_e due to changes in both d and y. Note especially that samples with the same d (same symbol) but different y (different shade) are consistent with the E_e dependence.

Interactions between dilute Mn spins and carrier spins are typically treated with a Kondo exchange Hamiltonian $H_{sp\text{-}d}=-\Sigma_i J_{sp\text{-}d}\sigma S_i$, where σ is the carrier spin, S_i is the spin of a Mn moment, and $J_{sp\text{-}d}$ is the exchange constant.[8] Direct Coulomb exchange contributes a positive (ferromagnetic) interaction to $J_{sp\text{-}d}$. Kinetic exchange due to virtual transitions between band states and localized d states causes an interaction that is equivalent (by a Schrieffer-Wolff transformation) to a negative (antiferromagnetic) exchange contribution to $J_{sp\text{-}d}$.[9,19] These virtual transitions, depicted in Fig. 5, typically dominate in the valence band where d levels strongly hybridize with the band-edge hole states, leading to antiferromagnetic coupling between the hole and Mn ion spins. In the conduction band, kinetic exchange vanishes at $\mathbf{k}=\mathbf{0}$ by symmetry,[1] leaving ferromagnetic direct exchange dominant.

This band-edge picture, supported by numerous magneto-optical measurements in bulk II-VI DMS, is inadequate for describing the reduced dimensionality of exchange in quantum-confined heterostructures. One approach to this situation is to treat the exchange constant $J_{sp\text{-}d}$ as $\mathbf{k}$-dependent within $\mathbf{k}\cdot\mathbf{q}$ theory, which leads to a reduction in the magnitude of valence-band kinetic exchange with increasing quantum confinement energy.[11] Though this model replicates the qualitative features of the data in II-VI materials, the prediction for the reduction of $N_0\alpha$ is a factor of ~5 smaller than what is observed in CdMnTe QWs.[10,11] In addition, this model amounts to a reduction of $|N_0\alpha|$ with increas-

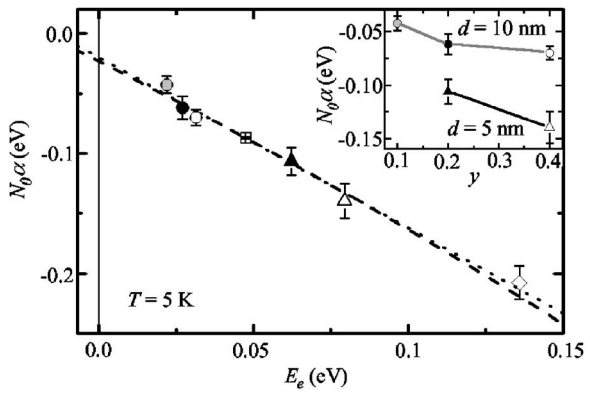

FIG. 4. $N_0\alpha$ plotted as a function of electron kinetic energy for QWs with $d=10$ nm (circles), $d=7.5$ nm (squares), $d=5$ nm (triangles), and $d=3$ nm (diamonds). $y=0.4$ (open symbols) are from Ref. 13, while $y=0.2$ (black) and $y=0.1$ (gray) are new to this manuscript. The dotted line is the linear approximation and the dashed line is an envelope function calculation based on Ref. 12. The inset compares $N_0\alpha$ for QWs of different barrier height y but the same width.

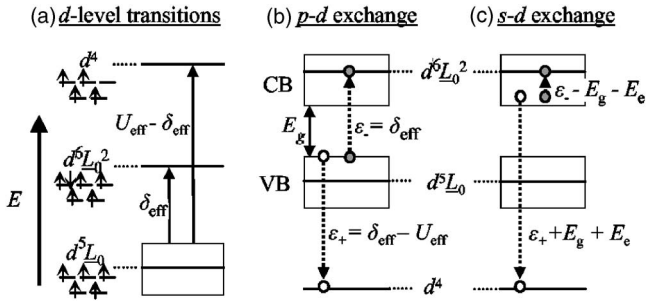

FIG. 5. (a) Schematic of the configuration-interaction model for core-level transitions from a d^5 Mn core with a valence-band hole ($d^5\underline{L}_0$) to a d^6 core with two valence holes ($d^6\underline{L}_0^2$) or a d^4 core. The effective parameters $U_{\text{eff}}-\delta_{\text{eff}}$ and δ_{eff} measure energies from the bottom of the core multiplet to the valence-band edge (Ref. 21). (b) The same core-level scheme shifted into a one-particle picture. The transitions between Mn core levels correspond to the electron and hole capture energies, ϵ_- and ϵ_+, responsible for valence-band kinetic exchange. (c) The corresponding scheme adjusted for kinetic exchange involving conduction-band electrons; $\gamma(E_e)$ in Eq. (1) corrects for the energy difference between the carriers in each scheme.

ing k, which is inconsistent with our findings in $Ga_{1-x}Mn_xAs$ QWs.

The negative shift in the antiferromagnetic $N_0\alpha$ observed in our experiments is better explained by a more complete model of the effects of reduced dimensionality accounting for the admixture of p-symmetry valence-band states and s-symmetry conduction-band states for nonzero $\mathbf{k}$ arising in $\mathbf{k}\cdot\mathbf{p}$ theory.[12] As quantum confinement increases electron kinetic energy (and thus k), the electron wave function takes on more p-symmetry character, increasing the antiferromagnetic contribution to $N_0\alpha$ from kinetic exchange. As Merkulov *et al.* point out,[12] depending on the degree of the admixture, a positive conduction-band exchange constant can decrease and even become negative with increasing kinetic energy.

We quantitatively apply the envelope function model of Ref. 12 to the data. To lowest order in E_e, the dimensionless slope of $N_0\alpha$ versus E_e is given by

$$\frac{d[N_0\alpha(E_e)]}{d|E_e|} = -\frac{2(E_g+\Delta)^2+E_g^2}{E_g(E_g+\Delta)(3E_g+2\Delta)}\left\{N_0\alpha_{\text{pot}} - [N_0\beta_{\text{pot}} + N_0\beta_{\text{kin}}\gamma]\left[1-\frac{4\Delta^2}{3[2(E_g+\Delta)^2+E_g^2]}\right]\right\}, \quad (1)$$

where Δ is the spin-orbit coupling, E_g is the band gap, $N_0\alpha_{\text{pot}}$ ($N_0\beta_{\text{pot}}$) is the direct conduction- (valence-) band edge exchange integral, and $N_0\beta_{\text{kin}}$ is the kinetic exchange integral of the valence band. The conduction-band kinetic exchange integral is assumed to be zero in the vicinity of $k=0$. γ is a parameter (see Ref. 12) that corrects the β_{kin} given by Schrieffer-Wolff kinetic exchange in the valence band for electrons in the conduction band. Valence-band potential exchange is assumed insignificant ($N_0\beta_{\text{pot}}=0$), but the model is sensitive to both the sign and magnitude of $N_0\beta_{\text{kin}}$. Since γ and $N_0\beta_{\text{kin}}$ were not measured directly in this experiment, we treat the product $\gamma N_0\beta_{\text{kin}}$ as a free fit parameter in the model. $N_0\alpha_{\text{pot}}$ is the only other free parameter in the model, appearing both in Eq. (1) and as the y intercept value of $N_0\alpha(E_e)$ at $E_e=0$. Equation (1) is generally insensitive to $N_0\alpha_{\text{pot}}$ since $N_0\beta_{\text{kin}}$ is typically an order of magnitude larger, so the extrapolation to $E_e=0$ determines the fit value for $N_0\alpha_{\text{pot}}$.

The linear fit to all sets of quantum wells using Eq. (1) is shown in Fig. 4 (dotted line). The best-fit results give $\gamma N_0\beta_{\text{kin}}=-2.28\pm0.19$ eV and the fit extrapolates to a bulk value of $N_0\alpha=-20\pm6$ meV. The value of γ is given by Ref. 12 in terms of the energies for virtual hole and electron capture in the Mn d levels, ϵ_+ and ϵ_-, respectively (Fig. 5). These can be estimated using a configuration-interaction analysis of core-level photoemission spectroscopy where the core ground state is assumed to be the Mn^{2+} ion [Fig. 5(a)].[21] The d^5 core and valence-band hole $\underline{L}_0$ hybridize with the $d^6\underline{L}_0^2$ state and the d^4 state,[22] leading to virtual transition energies in a one-particle picture of $\epsilon_+=-5.2\pm0.5$ eV and $\epsilon_-=2.7\pm0.5$ eV relative to the valence-band edge [Fig. 5(b)]. This analysis gives $\gamma=1.77$ for bulk $Ga_{1-x}Mn_xAs$, which allows us to estimate $N_0\beta_{\text{kin}}=-1.3\pm0.1$ eV from our linear fit.

$N_0\beta_{\text{kin}}$ has been measured previously in $Ga_{1-x}Mn_xAs$, and is influenced by the average electronic configuration of the Mn acceptors in the material. While $N_0\beta_{\text{kin}}$ has been found to be positive in uncompensated paramagnetic $Ga_{1-x}Mn_xAs$ with neutral Mn acceptors,[15,23] the MBE-grown samples studied here are compensated by Mn interstitials,[14] which act to ionize the Mn acceptors and cause a negative $N_0\beta_{\text{kin}}$.[24,25] The estimate $N_0\beta_{\text{kin}}=-1.3\pm0.1$ eV is consistent with previous results of MBE-grown $Ga_{1-x}Mn_xAs$ based on photoemission[21] and transport measurements[26] and from calculations.[27] This result is supported by direct measurements of a negative $N_0\beta_{\text{kin}}$ in multiple $Ga_{1-x}Mn_xAs$ QWs grown in the same conditions as the samples discussed here. As discussed in Refs. 13 and 14, magneto-PL cannot be used to accurately determine $N_0\beta$, but it can be determined by magneto-absorption.[28] The agreement between our estimate of $N_0\beta_{\text{kin}}$ obtained from the model and other measurements in MBE-grown $Ga_{1-x}Mn_xAs$ structures confirms the description of confinement-induced band mixing as an explanation for the variation of $N_0\alpha$ in the QWs.

Now we consider the nonlinear corrections to the linear approximation of Eq. (1). The nonlinear behavior enters through $\gamma(E_e)$, which accounts for the electrons sitting above the conduction-band edge and can be calculated for electrons away from $k=0$ according to Ref. 12 in terms of ϵ_+, ϵ_-, and E_e [Fig. 5(c)]. Using the values for ϵ_+ and ϵ_- and $N_0\beta_{\text{kin}}$ discussed above, we perform a more detailed calculation of the envelope function theory of Ref. 12 taking into account the E_e dependence in $\gamma(E_e)$ and yielding curvature at high E_e (Fig. 4). Because E_e is small compared to ϵ_- and ϵ_+, the curvature is too small to be directly observed by our measurements. Attempts to observe curvature at high E_e would be further complicated by the increased wave-function penetration into the $Al_yGa_{1-y}As$ barriers. Since the carrier virtual capture energies are not well known in $Al_yGa_{1-y}As$, reliable estimates of the effects of barrier penetration are not possible and calculations within this envelope theory are not adequate at high E_e. The good agreement between the model and the data support the conclusion that band mixing dominates the behavior *s-d* exchange as a function of 1D confinement en-

ergy in $Ga_{1-x}Mn_xAs$. While other treatments of kinetic exchange in QWs, such as the sp^3 tight-binding model,[20] are not excluded by this experiment, these models in their current form do not, to our knowledge, provide such numerical agreement in both II-VI and III-V DMS experiments.

Though accounting for the confinement effect, the above discussion does not address the extrapolation of our measurements to a bulk antiferromagnetic $Ga_{1-x}Mn_xAs$ exchange of $N_0\alpha=-20\pm6$ meV. This is an order of magnitude smaller than that typically measured in II-VI materials, and of the opposite sign. Its magnitude is similar to the +23 meV measured by Raman spin-flip scattering in $Ga_{1-x}Mn_xAs$,[29] but the sign is inconsistent with both previous measurements and band-edge *s-d* exchange theories. As in Ref. 13, this value of $N_0\alpha$ in bulk is an extrapolation. In an attempt to improve this extrapolation, the current experiment involves QWs with even lower confinement energy than in the earlier work. Direct measurements of bulk remain elusive as we have not yet found growth conditions that produce bulk $Ga_{1-x}Mn_xAs$ of high enough optical quality. Taking into account all of the QW systems measured, the best-fit value for $N_0\alpha$ is negative. While it is possible that our model does not extend to the bulk, the trend indicates a small and negative bulk $N_0\alpha$. We must therefore consider that some of the assumptions that are valid in II–VI do not apply in $Ga_{1-x}Mn_xAs$. For instance, because the Mn^{2+} ions replace Ga^{3+} in the lattice, they represent a repulsive Coulomb potential for the conduction-band electrons.[30] The resulting charge screening alters the overlap of Mn and carrier wave functions and is so far neglected in traditional calculations of *sp-d* exchange. The density of defects should be highly sensitive to growth conditions, leading to large variation in the charge screening and hence the measured values of the exchange constants.

In summary, we have extended earlier investigations into the kinetic energy dependence of *s-d* exchange in $Ga_{1-x}Mn_xAs/Al_yGa_{1-y}As$ QWs to include variations of both the QW width and barrier height. This relationship is found to be well fit by a band-mixing model where confinement-induced *p* symmetry in the conduction band causes an antiferromagnetic contribution to *s-d* exchange. The barrier height dependence of the kinetic exchange mechanism demonstrates that the exchange interactions in III–V magnetic heterostructures can be tuned using low-dimensional band engineering of quantum confinement.

We thank T. Dietl and J. A. Gaj for enlightening discussions and J. H. English and A. W. Jackson for MBE technical assistance. This work was supported by DARPA, ONR, and NSF. N.P.S. acknowledges support from the Fannie and John Hertz Foundation.

[1] T. Dietl, *(Diluted) Magnetic Semiconductors*, in *Handbook of Semiconductors*, edited by S. Mahajan (North-Holland, Amsterdam, 1994), Vol. 3B, p. 1251.
[2] D. D. Awschalom, J.-M. Halbout, S. von Molnar, T. Siegrist, and F. Holtzberg, Phys. Rev. Lett. **55**, 1128 (1985).
[3] S. A. Crooker, D. D. Awschalom, J. J. Baumberg, F. Flack, and N. Samarth, Phys. Rev. B **56**, 7574 (1997); S. A. Crooker, J. J. Baumberg, F. Flack, N. Samarth, and D. D. Awschalom, Phys. Rev. Lett. **77**, 2814 (1996).
[4] H. Ohno, A. Shen, F. Matsukura, A. Oiwa, A. Endo, S. Katsumoto, and Y. Iye, Appl. Phys. Lett. **69**, 363 (1996); H. Ohno, D. Chiba, F. Matsukura, T. Omiya, E. Abe, T. Dietl, Y. Ohno, and K. Ohtani, Nature (London) **408**, 944 (2000).
[5] R. C. Myers, K. C. Ku, X. Li, N. Samarth, and D. D. Awschalom, Phys. Rev. B **72**, 041302(R) (2005).
[6] J. A. Gaj, R. Planel, amd G. Fishman, Solid State Commun. **29**, 435 (1979).
[7] A. Twardowski, T. Dietl, and M. Demianiuk, Solid State Commun. **48**, 845 (1983).
[8] B. E. Larson, K. C. Hass, H. Ehrenreich, and A. E. Carlsson, Phys. Rev. B **37**, 4137 (1988).
[9] J. Blinowski and P. Kacman, Phys. Rev. B **46**, 12298 (1992).
[10] G. Mackh, W. Ossau, A. Waag, and G. Landwehr, Phys. Rev. B **54**, R5227 (1996).
[11] A. K. Bhattacharjee, Phys. Rev. B **58**, 15660 (1998).
[12] I. A. Merkulov, D. R. Yakovlev, A. Keller, W. Ossau, J. Geurts, A. Waag, G. Landwehr, G. Karczewski, T. Wojtowicz, and J. Kossut, Phys. Rev. Lett. **83**, 1431 (1999).
[13] R. C. Myers, M. Poggio, N. P. Stern, A. C. Gossard, and D. D. Awschalom, Phys. Rev. Lett. **95**, 017204 (2005).
[14] M. Poggio, R. C. Myers, N. P. Stern, A. C. Gossard, and D. D. Awschalom, Phys. Rev. B **72**, 235313 (2005).
[15] J. Szczytko, W. Mac, A. Stachow, A. Twardowski, P. Becla, and J. Tworzydlo, Solid State Commun. **99**, 927 (1996).
[16] K. Ando, T. Hayashi, M. Tanaka, and A. Twardowski, J. Appl. Phys. **83**, 6548 (1998).
[17] One-dimensional Poisson-Schrödinger solver written by G. Snider (http://www.nd.edu/gsnider/).
[18] B. Plot, B. Deveaud, B. Labert, A. Chomette, and A. Regreny, J. Phys. C **19**, 4279 (1986).
[19] J. R. Schrieffer and P. A. Wolff, Phys. Rev. **149**, 491 (1966).
[20] A. K. Bhattacharjee and J. Pérez-Conde, *Proceedings of the 25th International Conference on the Physics of Semiconductors*, edited by N. Miura and T. Ando (Springer-Verlag, Berlin, 2000), p. 242.
[21] J. Okabayashi, A. Kimura, O. Rader, T. Mizokawa, A. Fujimori, T. Hayashi, and M. Tanaka, Phys. Rev. B **58**, R4211 (1998).
[22] T. Mizokawa and A. Fujimori, Phys. Rev. B **56**, 6669 (1997).
[23] Th. Hartmann, S. Ye, P. J. Klar, W. Heimbrodt, M. Lampalzer, W. Stolz, T. Kurz, A. Loidl, H.-A. Krug von Nidda, D. Wolverson, J. J. Davies, and H. Overhof, Phys. Rev. B **70**, 233201 (2004).
[24] J. Szczytko, A. Twardowski, K. Swiatek, M. Palczewska, M. Tanaka, T. Hayashi, and K. Ando, Phys. Rev. B **60**, 8304 (1999).
[25] T. Weiers, Phys. Rev. B **73**, 033201 (2006).
[26] T. Omiya, F. Matsukura, T. Dietl, Y. Ohno, T. Sakon, M. Motokawa, and H. Ohno, Physica E (Amsterdam) **7**, 976 (2000).
[27] A. K. Bhattacharjee and C. Benoit à la Guillaume, Solid State Commun. **113**, 17 (2000).

[28] $N_0\beta$ is measured in multiple QW samples consisting of 100 8-nm GaAs quantum wells with 20-nm $Al_{0.4}Ga_{0.6}As$ spacers grown by the same MBE methods used to prepare the samples discussed here, described in Ref. 14. The heavy-hole exciton Zeeman splitting $\Delta E_{ex}=-g_{ex}\mu_B B$, where g_{ex} is the exciton g factor, is found from polarization-resolved reflectance measurements in the Faraday geometry on an undoped sample, while the sum of the exciton Zeeman splitting and the exciton exchange splitting, $\Delta E=\Delta E_{ex}+\Delta E_{sp-d}=-g_{ex}\mu_B B+xN_0(\alpha-\beta)\langle S_x\rangle$, is measured from Mn-doped multiple QWs with $x=0.001\,04$ as measured by SIMS. Fits to the exciton exchange splitting give $xN_0(\alpha-\beta)=1.48$ meV. KR measurement of $N_0\alpha$ allows extraction of $N_0\beta=-1.5\pm0.5$ eV, agreeing in sign and magnitude with the accepted literature values for MBE-grown $Ga_{1-x}Mn_xAs$.

[29] W. Heimbrodt, Th. Hartmann, P. J. Klar, M. Lampalzer, W. Stolz, K. Volz, A. Schaper, W. Treutmann, H.-A. Krug von Nidda, A. Loidl, T. Ruf, and V. F. Sapega, Physica E (Amsterdam) **10**, 175 (2001).

[30] C. Śliwa and T. Dietl, cond-mat/0505126 (unpublished).